



Technical Memorandum 80587

Energy Spectra of Cosmic Ray Nuclei to Above 100 GeV/Nucleon

{NASA-TM-80587} ENERGY SPECTRA OF COSMIC
RAY NUCLEI TO ABOVE 100 GeV/NUCLEON (NASA)
43 p HC A03/MF A01 CSCL 03B

N80-17011

Unclas
G3/93 11663

M. Simon, H. Spiegelhauer, W. K. H. Schmidt,
F. Siohan, J. F. Ormes, V. K. Balasubrahmanyam
and J. F. Arens

OCTOBER 1979

National Aeronautics and
Space Administration

Goddard Space Flight Center
Greenbelt, Maryland 20771



Energy Spectra of Cosmic Ray Nuclei to Above 100 GeV/Nucleon

M. Simon**, H. Spiegelhauer, W. K. H. Schmidt[†]
Max Planck Institute für Extraterrestrische Physik
8046 Garching, Federal Republic of Germany

F. Siohan*, J. F. Ormes, V. K. Balasubrahmanyam, J. F. Arens
NASA/Goddard Space Flight Center
Greenbelt, Maryland 20771 USA

ABSTRACT

Energy spectra of cosmic ray nuclei boron to iron have been measured from 2 GeV/nucleon to beyond 100 GeV/nucleon. The data were obtained using an ionization calorimeter flown on a balloon from Palestine, Texas. The 3450kg payload floated at 7g/cm^2 for almost 24 hours. The results are in excellent agreement with those of other workers where overlaps exist. The spectra are not consistent with single power laws, and demonstrate the power of using a single technique sensitive over a large dynamic range. The data are consistent with the leaky box model of cosmic ray propagation. The boron data indicate that the cosmic ray escape length decreases with increasing energy as $E^{-(0.4\pm 0.1)}$ up to 100 GeV/nucleon. Secondary nuclei from iron are also consistent with this dependence. Predicted changes in the energy dependence of the ratios of primary nuclei O/C and IRON/C+O are also observed.

**Now with University of Siegen, Federal Republic of Germany

[†] Now with Max Planck Institut für Aeronomie, Federal Republic of Germany

* NAS/NRC Resident Research Associate, now with Oxford University, England

1. Introduction

All nuclei of the periodic table of the elements are present in the cosmic radiation and the comparison between the relative abundance of cosmic ray nuclei and the "the universal abundance" provides information about their origin and propagation through interstellar space. Interest in these studies has increased since experimental results indicated that the relative abundance of cosmic ray nuclei is energy dependent. These results have led to a very lively discussion concerning the understanding of the cosmic ray confinement mechanisms in the galaxy and interstellar propagation. These observations provide clues in the study of the distribution of path lengths through which the particles pass in the galactic containment region. The mean interstellar matter traversed can be studied by comparing the ratios of the secondary to primary components. Observations show that at high energies the particles traverse less interstellar matter than at low energies indicating that the cosmic ray source composition is less subject to corrections at high energies. For this reason much effort has been devoted in the last few years to the development of high energy cosmic ray experiments, and many nuclear species have now been observed at energies up to 100 GeV/nucleon. These results were obtained employing instruments such as ionization spectrometers (Balasubrahmanyam and Ormes, 1973, Saito et al., 1974, and Schmidt et al., 1976), gas Cherenkov counters (Juliusson, 1974 and Caldwell, 1977, Lezniak and Webber, 1978) and magnetic spectrometers (Orth et al., 1978). Based on these data, a variety of interpretations were possible, and there were some differences between different techniques.

In this paper the results of the chemical composition of cosmic rays as a function of energy in the range of a few GeV/nucleon to some hundreds of GeV/nucleon for boron through iron are presented. The experiment combined an

ionization spectrometer and a gas Cherenkov counter to perform two different and independent energy measurements. This combination also provided for the first time an experimental cross-check on the response of both types of detectors to heavy nuclei.

In all these balloon-borne experiments the major constraint in extending the energy range is the low flux of cosmic ray nuclei at high energies. This requires experiments with large area solid angle factors. In order to maximize the statistical significance of the results, the experiment was optimized for collection area at the expense of both charge and energy resolution. Much of this paper is devoted to a discussion of how the resulting problems are handled so that the critical reader can evaluate these results. A price was paid in terms of the increased background, which had to be evaluated carefully.

The experiment was successfully flown in October 1976 from Palestine, Texas, at a mean altitude of 7 g/cm² residual atmosphere, providing a total exposure of 15.5 m² ster hr. The weight of the scientific payload was 2653.6 kg and the total suspended payload was 3450 kg.

2. Experimental Apparatus

A detailed description of the experimental apparatus has been published (Arens et al., 1979). Here, a short description of the major components will suffice. Figure 1 shows the experimental configuration. This apparatus consisted basically of three parts:

- 1) a gas Cherenkov counter on top of the instrument with an energy threshold of 16.5 GeV/nucleon,
- 2) five organic scintillators (Pilot Y) and a solid Cherenkov counter (Pilot 425) which measured charge and trajectories, and
- 3) an ionization spectrometer or calorimeter for energy determination.

The sensitive area of the apparatus as defined by the upper scintillator was 1.2m x 1.2m and the geometric factor was 0.72m² ster, which reduced to

0.28m² ster for those particles which penetrated both the gas Cherenkov counter and the spectrometer. For the balloon flight, the instrument was placed in a styrofoam housing for thermal insulation. Due to the large size of the instrument no pressurized gondola was used.

The compromise to launch a large payload without a picture device (without a pressurized gondola, no gas filled device such as spark chambers or multiwire proportional counters could be used) created a background problem. Events with a large number of particles, especially due to air showers at large zenith angles produced a background which is unusual for experiments of this kind. The method of handling this background will be discussed in section 5.

The combination of the gas Cherenkov counter with the ionization spectrometer in this experiment provided a means of cross checking the response characteristics of both detector systems to heavy nuclei. The response of the ionization spectrometer to the different heavy cosmic ray nuclei could be calibrated with the threshold and response of the gas Cherenkov counter; the response distribution of the gas Cherenkov counter could be checked for the effects of residual scintillation light by using the spectrometer for energy cuts. These points are discussed in section 4 and in more detail in a separate paper (Balasubrahmanyam et al., 1979).

The properties and the limitations of the position sensing scintillator technique for determining the trajectories in this high energy cosmic ray experiment are discussed in the instrument paper (Arens et al., 1979). The basic idea behind this technique is simple: one locates the position of incidence by exploiting the fact that the measured signal depends on the location in the scintillator relative to the phototubes. Since the pulse height measurements are subject to photoelectron fluctuations, this technique is most useful for heavy cosmic ray nuclei. The position of an incident particle

could be located to within a few centimeters in the different detectors and was adequate for our purposes; however, the resulting inaccuracy in the trajectories did in fact limit the charge resolution. At high energies the charge resolution was further hampered by backscatter effects, and multiple tracks could not be detected easily, points which will be discussed further.

3. Charge Determination

The charge determination was performed with five independent charge detectors, i.e. the four scintillators S1x, S1y, S3x, S3y and a solid Cherenkov counter. Since the Cherenkov counter was viewed by two sets, each of 4 phototubes, a total of six charge signals were available. Zenith angle corrections and corrections for the spatial non-uniformity of light collection were applied to all the charge detectors. A series of scatter plots were then constructed from the flight data in which each scintillator was compared with the Cherenkov response. The curves through the charge peaks in these two dimensional plots, representing the charge lines, were constructed by a best fit technique. By using all the detectors, a six-dimensional distribution of data and the corresponding charge line was obtained.

An individual cosmic ray event was attributed to the charge corresponding to the nearest point, measured in units of σ_i , on the charge line, i.e. by minimizing the expression

$$\chi^2 = \sum_{i=1}^n \cdot \frac{(X_L^i - X_p^i)^2}{\sigma_i^2} \quad (1)$$

Here, the x_L^i are the coordinates of the position on the charge line to be found, and the x_p^i are the charge coordinates of the event considered. The sum extends over all the charge coordinates used and each term is weighted by the corresponding charge signal variance σ_i^2 . The charge variable was thus effectively

treated as continuous. The line position was then projected onto the Cherenkov axis for an absolute analog charge measure. The Cherenkov axis was chosen, since no saturation in the signals up to iron nuclei was found, thus yielding a strictly Z^2 -proportional charge measure. The above procedure of determining the charge avoided any scale adjustment, since the charge line took into account the individual response of each detector. The absolute value of the minimum χ^2 also provided a measure of the acceptability of an event. Note, however, that this variable is not expected to obey a classical χ^2 distribution because of the non-Gaussian signal fluctuations and a certain degree of correlation among the detector signals.

In the course of the analysis it was observed that the mean pulse height for each charge tended to increase systematically with energy as illustrated in Figure 3. The rate of signal increase is more pronounced the closer the detector is located to the spectrometer. This behavior is attributed to relatively low energy particles which flow back from the iron spectrometer. These particles then stop preferentially in the detector close to the spectrometer. The increases in SIX and SIY, the detectors which are further away, are quantitatively consistent with being caused by δ -ray production between 1 and 20 GeV/nucleon (Yodh, 1977). Because of the backscatter, only SIX, SIY and the two sets of PMTs from the solid Cherenkov-detector have been used, and the χ^2 values should correspond to 3 degrees of freedom. Fig. 2 shows a charge histogram for particles in the energy range 20 to 40 GeV/nucleon obtained by accepting all events with χ^2 - values smaller than 10 and a comparable background histogram for χ^2 values between 36 and 100. (A discussion of handling events in the χ^2 range 10-35 is deferred until section 5.) The more plentiful species (B, C, O, Ne, Mg, Si, Fe) stand out conspicuously and the

charge resolution is about 0.4 charge units around oxygen and 1.6 charge units around iron. The detector resolution (σ) was about 10% independent of charge and was limited by the accuracy with which the trajectories of an incident particle could be determined. Because individual element resolution has not been obtained, the elements have been grouped together as indicated in the figure. Because nitrogen lies between the abundant carbon and oxygen and does not clearly stand out, spectra for this nucleus should be considered cautiously. The boron peak appears to stand out in all the plots and so those results are included. The separation of boron from the abundant background will be discussed later. Note how steeply the background decreases as a function of increasing charge.

The signal resolutions σ_i 's in equation 1 taken for the four detectors SIX, SIY and the two sets of Cherenkov tubes were respectively 7, 5, 7 and 9 percent. They were obtained by a subset of the carbon and oxygen nuclei which penetrated the central regions of the detectors. We found them to be independent of charge. We assumed that they are independent of energy. This might lead to a slight underestimation of σ 's at high energies, but as will be shown later, an independent decision is made about the background correction for each charge and energy bin, taking account of any variation. An incident iron nucleus which strips off an alpha particle at the bottom of SIY and hence registers as a chromium in the Cherenkov detector would, in the absence of other fluctuations give a χ^2 value of 9 and lies at the limit of our detection. An iron that fragments into a calcium on the other hand, would give a χ^2 value greater than 50 and is easily rejected. An allowance is made for the undetected interactions when the correction is made for interactions in the telescope.

4. Energy Determination

The principal detector for determining the energy of the cosmic ray nuclei was the ionization spectrometer (Fig. 1). A primary particle converts a substantial part of its initial kinetic energy into a nuclear electromagnetic cascade.

The cascade builds up by a series of nuclear interactions in the spectrometer. Energy is measured by sampling the resultant electromagnetic cascades at various depths in the absorber. In this experiment the iron slab scintillator sandwich was divided into three modules. Each module was viewed from two opposing sides by phototubes at the ends of air light guides with white walls. A vertically incident cosmic ray encounters a total of 170 g/cm^2 iron plus 5.9 g/cm^2 scintillator material, which corresponds to 1.44 proton and about 6 iron nuclear interaction lengths.

For an infinitely deep calorimeter the SUM signal from all the scintillator samples is proportional to the kinetic energy of the incident nuclei no matter where the first interaction within the calorimeter takes place. All the energy is absorbed and the signal distribution would be Gaussian in shape and have a resolution of about 10%. However, in this finite thickness device, the fraction of the primary energy deposited is dependent upon the location and characteristics of the first interaction, resulting in a broad SUM signal distribution. A thorough discussion concerning this effect on the shape of a measured cosmic ray spectrum is given in an earlier paper, Jones et al, (1977). In this analysis we utilize the fact that the cascade develops differently depending on the location of the first interaction in order to improve the resolution

The gas Cherenkov counter has been used to provide a calibration for this purpose. Fig. 4 shows the response of the gas Cherenkov counter for oxygen nuclei as a function of the calorimeter signal. No restrictions have been placed on the calorimeter signals but data have been selected to have trajectories passing through the gas Cherenkov counter and to have consistent signals in the two banks of PMT's. At low calorimeter signal levels the finite response in the gas Cherenkov counter is due to the scintillation in the Freon gas. As the energy of particles can be identified in this experiment using the calorimeter, this scintillation level is determined explicitly. Consequently the threshold of the gas Cherenkov

counter can be determined quite accurately minimizing the uncertainty due to the scintillation contribution of the gas Cherenkov counter. The curve shown in Fig. 4 is based upon the energy determined from Equation 2, described below. Similar plots are obtained for other nuclei. From these plots the charge independence of the calorimeter signal (on a per nucleon basis) corresponding to the threshold of the gas Cherenkov counter is demonstrated as seen in the insert in Fig. 4.

Plots of the gas Cherenkov response as a function of the calorimeter signal can also be made for given Fe1 signals. In this manner, the correlation of the calorimeter SUM signal with the Fe1 signal can be found. This correlation is indicated by the data points in Fig. 5. In addition to this experimental check, Monte Carlo simulations (Jones, 1976 and Jones et al, 1977) have been used to deduce the correlation for other energies. An empirical fit was found which is well represented by the following expression:

$$E = 0.218 \frac{(\text{SUM})^{1.36}}{(\text{Fe } 1)^{0.38}} \quad (\text{GeV/nucleon}). \quad (2)$$

The lines in Fig. 5 are for constant energy as computed by this formula. The term $\text{SUM}^{1.36}$ has the effect of allowing for the increasing fraction of energy escaping out the bottom of the calorimeter as the energy increases, and the term $\text{Fe}1^{-0.38}$ compensates for what happens in the first interaction. Note that when the SUM and Fe1 signals are expressed in particles per incident nucleon, this expression is independent of charge. The Monte Carlo calculations and the gas Cherenkov data gave consistent values for the constant which represents the energy calibration. Thus, at 16.5 GeV/nucleon our energy scale has been determined to within 5% and is independent of charge. At other energies, since we depend on the Monte Carlo simulation, an increased energy scale error is allowed because of the distance from the gas Cherenkov calibration point. These estimated errors are summarized in Fig. 6.

An example of how equation 2 fits the Monte Carlo simulation is shown in Fig. 7 for 100 GeV/nucleon carbon. The clump of particles in the lower left hand corner of the plot have penetrated deeply into the calorimeter and are lost for energy determination. A correction for this effect is discussed below. The simulations show some Z dependent effects at low energies (1-3 GeV/nucleon) which may indicate slight problems with the Monte Carlo program at energies where ionization loss effects are important. Therefore only data for energies $E \geq 2.5$ GeV/nucleon are analyzed.

Observed energy distributions for Monte Carlo simulated data are shown in Fig. 8. Simulated monoenergetic incident carbon nuclei of 30 GeV/nucleon are analyzed by two different methods. The solid histogram shows the distribution obtained by taking the SUM signal and the dashed histogram shows the improvement obtained by applying the equation (2). The dashed histogram peaks more sharply around 30 GeV/nucleon although both distributions extend to near zero for those particles which penetrated deeply before interacting.

The Monte Carlo events provide a series of distributions which can then be used to deconvolve the energy spectra. Because of the power law nature of the energy spectra the slopes are not very sensitive to these deconvolutions. This is true as long as the shape of the response distribution varies slowly with energy (Jones et al., 1977). On the other hand, the intensities must be corrected for the spillage from bin to bin. For example, particles which penetrate deeply into the calorimeter with little or no interaction are lost. They appear as low energy particles, and because of the steeply falling cosmic ray spectrum they have a statistically significant effect only when they fall in the next lower energy bin. Particles which fall into the next higher energy bin are few in number but their effect is enhanced by the cosmic ray spectrum. In order to

deduce the correct fluxes Monte Carlo simulated distributions for carbon, silicon and iron nuclei at 3, 6, 17, 30 and 100 GeV/nucleon were used. Energy bins were overlaid on these plots, and the events lost and those going into adjacent bins were counted. By allowing both for the events lost and gained, appropriately weighted by the spectrum, a correction was derived. Fig. 9 shows the multiplicative correction factor (CE) derived. At low energies nuclei stop by ionization loss so the correction factor is 1, but at higher energies particles can penetrate deeply without interacting or by suffering low multiplicity interactions. The net result is a slight flattening of the observed spectra. Uncertainties in these deconvolution corrections are based on the statistical significance of the Monte Carlo runs and are indicated in Fig. 9. This error has been included in the quoted flux and dominates at all but the highest energies where statistical errors dominate. In taking ratios of intensities the effect of these convolution corrections tend to cancel.

5. Background

Because of the large area of the experiment and the lack of a trajectory picture device, a substantial background of multiple particles exists, apparently due to air showers, mostly from large zenith angles. Most of these events lie at large χ^2 values (see equation 1 and the discussion of the charge analysis) indicating that their pulse height were inconsistent in the SIX, SIY and the Cherenkov detectors. However, the low χ^2 tail of the distribution can simulate good events. The background falls off rapidly with increasing charge but because it has an "apparent" spectrum which is considerably flatter than that of "real" events, is troublesome for low Z particles at high energies. A background event usually gives a trajectory (which measures the "center of gravity" of particles) which is reasonable and so this cannot be used to reject these events. In summary,

the relative amount of background is both charge and energy dependent. The method of determining the flux of particles in a given charge and energy bin is illustrated in Figure 10. The open circles indicate the χ^2 distribution for all carbon nuclei in the bin centered at 15.8 GeV/nucleon. Below $\chi^2 = 10$, the distribution is dominated by good events with resolved charges. At high χ^2 , beyond 36, the distributions show no evidence of charge resolution and the distribution is clearly dominated by background. The problem is to determine what to do in the transition between where there is an admixture of background and good events, and to find an effective cut that properly estimates the background. To do this, a χ^2 distribution consisting predominantly of background was constructed, based upon the shape of the cascades in the calorimeter. For legitimate downward moving high energy particles, cascades should build up with increasing depth (e.g. Fe 3 signal > Fe 2 > Fe 1). It was observed that events for which this condition was violated had indeed mainly high χ^2 values. Therefore, by selecting events for which a major fraction of the energy was deposited in Fe 1, a χ^2 distribution was formed for background events for each charge and energy bin. The example shown in Figure 10 by the solid circles is typical, and the shapes (for background) were nearly independent of energy. The background distribution is then normalized to the all particle distribution at large χ^2 values and the flux of good events is found by a subtraction of two distributions. An effective cut can also be defined which gives the same intensity. At lower energies, the peak to valley ratios are pronounced (10:1), and the cuts are obvious and typically occur at χ^2 values of 30. A sequence of examples is shown in Figure 11 for boron, carbon and iron secondary nuclei in the energy intervals indicated. The error in this procedure is comparable to the statistical error and has been included in the quoted errors.

6. Interaction Corrections

A correction is made for the interactions in the 2.57 g/cm^2 of Al and the 1.28 g/cm^2 of scintillators at the top of the instrument. The interaction mean free paths and the corrections used are given in Table 1. The correction factor is adjusted for the fraction of interactions which can be detected by the χ^2 techniques used. For example, in the case of iron secondaries ($17 \leq Z \leq 20$) the correction factor would be 1.43, but since only 2/3 of the interactions are detected, this reduces to $(1 + 2/3 \times .43) = 1.29$. The factor 2/3 comes from the partial cross sections for interactions which go undetected, i.e. 1 in 3 interacting nuclei do not change charge by enough to raise their χ^2 sufficiently to be rejected.

To correct the fluxes obtained to the top of the atmosphere, a full propagation analysis has been done and growth curves derived. The mean free paths used are also shown in Table 1. For boron and iron secondaries, a range of values is given, because the correction depends on the abundance ratio (to carbon and iron respectively) observed; the smaller the observed abundances, the larger the fraction which has been produced in the atmosphere. The quoted errors indicate the range of values used for these data. This correction becomes very important at high energies where the interstellar material traversed is less (at $100 \text{ GeV/nuc} \approx 1 \text{ g/cm}^2$) and more than half of the observed flux is atmospherically produced.

7. Results and Conclusions

The derived fluxes of all the components at the top of the atmosphere are given in table 2. Results for oxygen and iron nuclei, multiplied by $E^{2.5}$ power to emphasize the spectral structure, are shown in Figure 12 along with some of the recent data from other groups. The agreement between the different measurements is quite good and generally within the quoted errors. The oxygen data of Lezniak and Webber (1978) seem to be slightly lower than those of the other groups, e.g. the Orth et al. (1978) data and those of the Chicago group (Juliusson, 1974 and Caldwell, 1977).

The spectra derived from this experiment are shown in figure 13, again multiplied by $E_K^{2.5}$ power. The spectra are given as functions of kinetic energy. The oxygen data span almost 3 decades in energy (corresponding to 7 decades in intensity). The low energy data, (2-20 GeV/nucleon) when plotted as a function of total energy $\times E_T^{2.5}$, are quite flat; but the data at high energy indicates that there is a gradual steepening of the spectra. For example, between 2 and 20 GeV/nucleon the iron data is fitted by $E_K^{-2.2}$ while the highest energy data is consistent with $E_K^{-2.7}$. The results agree with spectra derived using a thicker calorimeter (Balasubrahmanyam and Ormes, 1973) and with gas Cherenkov counters (Juliusson, 1974, Caldwell, 1977) when allowance is made for the different energy coverage of the different experiments. It should be noted that the statistics are not sufficient to rule out the iron spectrum Goodman et al. (1979) require to explain their observations of delayed particles at mountain altitudes. Their result at 2-20 TeV/nucleon indicate an iron spectrum as flat as $E^{-2.36 \pm 0.06}$ from 10 GeV/nucleon onwards.

In Figure 14 the experimental B/C+O ratio is shown along with the best fit power law dependence of the mean escape length, $\lambda_e = 9 \text{ g/cm}^2 (E/\text{GeV/nuc})^{-(0.4 \pm 0.1)}$. The calculation is based upon an exponential distribution of vacuum path lengths in the phenomenological leaky box model for cosmic ray propagation. The interaction mean free paths used for the propagation calculation, including the effect of 10% He, are given in the last column of Table 1. (See Ormes and Freier 1978 and references therein for a discussion of the propagation model). This mean escape length has been allowed to vary with energy in the manner indicated in order to fit to the data in the energy range of this experiment. This energy dependence of the mean escape length is consistent within errors of those previously

derived (Caldwell, 1977, Lezniak and Webber 1978 and Orth et al. 1978) Because of the competition between escape and interaction loss mechanisms, ratios between primary nuclei also vary in this model. In Figure 15 and 16 the O/C and the iron/C+O ratios are shown, again compared with the expected ratios as a function of energy. The λ_e has the same form as fitted to the B/C+O data, and the source ratios are taken from Shapiro et al. (1975). A 10% higher source abundance of O would fit the O/C ratio and the IRON/C+O ratios better. The larger source ratio of iron derived by Lezniak and Webber (1978) is not indicated by these data.

Finally in Figure 17 the ratio of iron secondaries ($17 < Z < 25$) to iron nuclei is shown along with the results from other workers. Our high energy data tend to fall below the predicted ratios, especially in the energy range 3-30 GeV/nucleon. The predicted ratios have been calculated based upon a cross section for fragmentation of iron into ($21 < Z < 25$) of 411 mb. The higher ratio observed around 1 GeV/nuc by Lezniak and Webber (1978) probably reflects the increase in the cross section towards lower energy. The sub-iron nuclei can be used to probe the shape of the cosmic ray path length distribution. Various workers (Lezniak & Webber, 1979, Garcia Munoz et al., 1977) studying cosmic rays below 1 GeV/nucleon have suggested that the sub-iron abundances are large enough that the path length distribution must be truncated below 1 g/cm² (Shapiro et al., 1973). Since the cross sections and especially their energy dependence in the range 1 to 10 GeV/nucleon are not adequately known, it is difficult to draw any conclusions about the cosmic ray path length distribution based upon these data. However, since truncation of the cosmic ray path length distribution will increase the number of iron secondaries predicted, it is difficult to see how our data can be consistent with any truncation. Further measurements of the cosmic ray intensity above the atmosphere and better determination of the energy dependence of the cross sections of the energy range 1-10 GeV/nucleon will be required to resolve this question.

In conclusion, the data are all consistent with a quite simple propagation model in which the escape of cosmic rays from the galaxy is energy dependent. At high energies (>50 GeV/nuc) the uncertainties in the atmospheric corrections are important and indicate the need for satellite measurements. At around 100 GeV/nucleon the cosmic rays observed at earth are almost an order of magnitude younger than those at 1 GeV/nucleon and more nearly reflect the source composition. When high statistics observations of the nuclei in the charge range $9 \leq Z \leq 25$ are made above the atmosphere at 100 GeV/nucleon the source composition of these rare components can be determined.

Acknowledgements

We would like to thank Dr. F. B. McDonald and Dr. K. Pinkau for their support and encouragement. Mr. C.R. Greer, Mr. G. Cooper and Mr. A. Puig helped to build and test the detectors under the able supervision of Mr. J. Laws who provided electrical engineering support. This experiment was also supported by the Bundesminister fur Forschung and Technologie of Federal Republic of Germany under the title WRK244 and WRK275:5. Also thanks are due to the excellent launch and support provided by the crew of the National Scientific Balloon Facility at Palestine, Texas for launching this payload which set a record for weight carried above 100,000 feet on a balloon.

We would also like to thank an anonymous referee for carefully reading the manuscript and providing us with several helpful suggestions.

AUTHORS NAMES AND ADDRESSES

Dr. Manfred Simon
University of Siegen
Federal Republic of Germany

Dr. H. Spiegelhauer
Max Planck Institut für Extraterrestrische Physik
8046 Garching
Federal Republic of Germany

Dr. W. K. Schmidt
Max-Planck-Institut für Aeronomie
3411 Katlenburg-Lindau 3
Federal Republic of Germany

Dr. F. Siohan
Oxford University
England

Dr. J. F. Ormes and Dr. V. K. Balasubrahmanyam
Code 661
NASA/Goddard Space Flight Center
Greenbelt, MD 20771 U.S.A.

Dr. J. F. Arens
Code 690
NASA/Goddard Space Flight Center
Greenbelt, MD 20771 U.S.A.

TABLE 1

<u>CHARGE</u>	<u>MFP* IN ALUMINUM</u>	<u>MFP* in SCINTILLATOR</u>	<u>Correction for interacting events rejected</u>	<u>MFP* in AIR</u>	<u>Atmospheric⁺ Correction</u>	<u>MFP* in ISM (10% He)</u>
5	43.2	21.3	1.20	27.5	.76-.96	6.6
6	40.1	20.0	1.22	26.2	1.25	6.2
7	37.2	18.6	1.23	24.0	1.22	5.6
8	34.7	17.5	1.26	22.7	1.32	5.1
10	30.8	15.7	1.29	20.8	1.23	4.4
12	27.8	14.4	1.33	10.4	1.34	3.9
14	25.6	13.3	1.36	18.2	1.40	3.52
10<Z<16			1.33		1.34	
17<Z<20			1.29		0.86-1.00	
21<Z<25			1.31		0.62-0.93	
26	19.8	9.3	1.43	13.5	1.44	2.2

*MFP = mean free path for interaction in g/cm²

⁺At mean slant depth of 7.5 g/cm²

TABLE 2
(Fluxes in Particles/m²sr sec GeV/nuc)
 $(X \pm \Delta X) \cdot 10^{-N} \equiv (X \pm \Delta X) \times 10^{-N}$

Energy GeV/Nucleon	Boron	Carbon	Nitrogen	Oxygen	10<Z<16	17<Z<20	21<Z<25	26<Z<30
2.5	0.17±.03	0.68±.1	0.25±.04	0.66±.09	0.48±.07	(2.6±.4) ⁻²	(1.5±.3) ⁻²	(5.8±0.9) ⁻²
4.0	(7.7±1.2) ⁻²	0.27±.04	0.11±.02	0.29±.04	0.22±.03	(1.2±.2) ⁻²	(8.2±1.3) ⁻³	(3.0±.4) ⁻²
6.3	(2.0±.3) ⁻²	(9.4±1.4) ⁻²	(3.4±.5) ⁻²	0.10±.013	(7.9±1.2) ⁻²	(4.5±.7) ⁻³	(3.0±.5) ⁻³	(1.3±.2) ⁻²
10.	(5.6±.1) ⁻³	(3.5±.5) ⁻²	(1.2±.2) ⁻²	(3.8±.5) ⁻²	(2.8±.4) ⁻²	(1.7±.3) ⁻³	(1.0±.2) ⁻³	(4.2±.7) ⁻³
16.	(1.8±.3) ⁻³	(1.2±.2) ⁻²	(3.7±.6) ⁻³	(1.3±.2) ⁻²	(.99±.15) ⁻²	(5.0±.8) ⁻⁴	(3.5±.6) ⁻⁴	(1.6±.3) ⁻³
25.	(7.9±1.2) ⁻⁴	(3.7±.5) ⁻³	(1.1±.2) ⁻³	(4.5±.7) ⁻³	(2.9±.4) ⁻³	(1.4±.3) ⁻⁴	(1.1±.2) ⁻⁴	(4.8±.9) ⁻⁴
40.	(1.5±.5) ⁻⁴	(1.1±.2) ⁻³	(2.7±.5) ⁻⁴	(1.3±.2) ⁻³	(.95±.15) ⁻³	(5.3±1.1) ⁻⁵	(3.7±.8) ⁻⁵	(1.9±.4) ⁻⁴
63.	(4.0±1.4) ⁻⁵	(2.5±.5) ⁻⁴	(7.4±2.) ⁻⁵	(3.3±.5) ⁻⁴	(3.0±.5) ⁻⁴	(1.2±.4) ⁻⁵	(1.0±.3) ⁻⁵	(3.9±1.2) ⁻⁵
100.	(1±.4) ⁻⁵	(8.0±.1) ⁻⁵	(1.8±.6) ⁻⁵	(1.3±.3) ⁻⁴	(.91±.2) ⁻⁴	(6.5±2.3) ⁻⁶	(2.7±1.1) ⁻⁶	(4.6±3.) ⁻⁶
160.		(2.9±.4) ⁻⁵	(3.9±2.) ⁻⁶	(1.8±.4) ⁻⁵	(2.4±.5) ⁻⁵	(1.3±.8) ⁻⁶	(7.6±4) ⁻⁷	(6.9±3) ⁻⁶
250.		(4.4±1.3) ⁻⁶	(4. ± 4) ⁻⁷	(5.9±1.3) ⁻⁶	(.81±.2) ⁻⁵			(2.6±2) ⁻⁶
400.		(1.8±.8) ⁻⁶		(3.2±1.0) ⁻⁶	(1.7±.7) ⁻⁶			
630.		(6.1±.4) ⁻⁷		(1.2±.5) ⁻⁶	(5.4±3) ⁻⁷			
1000.				(2.2±1.3) ⁻⁷	(1.2±1.2) ⁻⁷			

FIGURE CAPTIONS

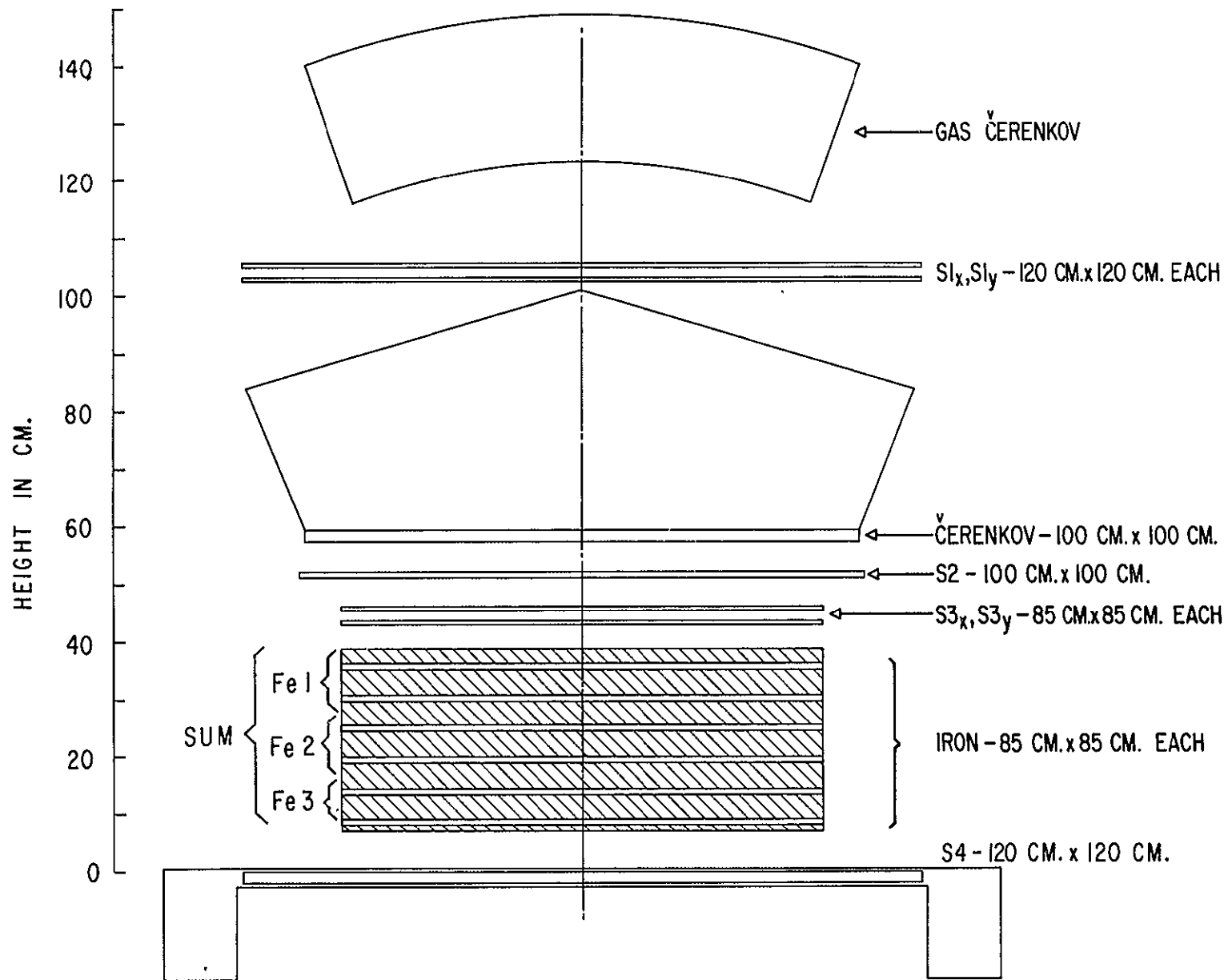
1. Schematic diagram of the instrument.
2. Charge histograms for particles between 20 and 40 GeV/nucleon. The upper curve is for good events, and the lower curve is for background events as selected by the consistency of measurements in the charge detectors.
3. Mean response of charge detectors as a function of energy. S_{3x} and S_{3y} are detecting backscattered energy from the calorimeter and hence are not used in the charge analysis.
4. A cross plot of the gas Cherenkov detector and the calorimeter for oxygen nuclei. Such plots are used to check the calibration of the calorimeter in the Monte Carlo simulation. The insert shows this calibration for different incident nuclei, confirming its independence of charge.
5. This curve shows lines of constant energy on a SUM vs. Fe 1 crossplot. The background region is where events fall which have cascades which develop too fast in the calorimeter. The data points indicate the calibration from the gas Cherenkov threshold based on in-flight oxygen nuclei.
6. The estimated energy uncertainty as a function of energy.
7. Calorimeter response cross plot from the Monte Carlo simulations of 100 GeV/nucleon carbon nuclei. The solid curve represents the calibration curve for 100 GeV/nucleon particles.
8. The solid curve shows the calorimeter SUM response distribution for 30 GeV/nucleon Monte Carlo simulated carbon events. The dashed curve shows the distribution of observed energies when corrected for the Fe 1 pulse height and the energy escaping out the bottom using equation 2.
9. Multiplication factors which account for energy bin spillover effects. Primarily these particles have penetrated too deeply in the device to have their observed energy within the resolution bin.

10. An example (15.8 GeV/nucleon carbon nuclei) to illustrate the procedure for subtracting background. The background (filled circles) distribution comes from events in the cross hatched region of Figure 5.
11. Several examples for different charges and energy bins of the χ^2 distributions and the renormalized background distributions. Fluxes are obtained by subtracting these two distributions.
12. The oxygen and iron spectra as determined from this experiment (solid circles) compared with measurements of other values. The spectra have been multiplied by $E^{2.5}$ (kinetic energy) to emphasize differences. The intensities are in particles/m² sr GeV/nuc and kinetic energy is in GeV/nuc. The open squares are due to Orth et al. (1978), the open circles to Caldwell (1977), the crosses to Juliusson (1974), and the vertical lines to Lezniak and Webber (1978).
13. The spectra of various components as determined from this experiment multiplied by $E^{2.5}$ (kinetic energy) to emphasize spectral features. The intensities are in particles/m² sr GeV/nuc and kinetic energy is in GeV/nuc.
14. The boron to carbon plus oxygen ratio from these measurements compared to mean escape lengths calculated as a function of the energy dependence indicated.
15. The same calculation (see Figure 14) compared to the O/C ratio data. The source ratios are taken from Shapiro et al., 1975.
16. The same calculation (see Figure 14) applied to the IRON GROUP/C+O ratio data.
17. The ratio of iron secondary nuclei to iron nuclei compared to the data of other workers. The symbols are as follows: G, Garcia-Munoz et al., 1977; L, Lezniak and Webber, 1978; C, Caldwell, 1977; J, Juliusson, 1974; O, Orth et al., 1978; and Solid Symbols represent this work.

REFERENCES

- Arens, J. F., Balasubrahmanyam, V. K., Ormes, J. F., Siohan, F., Schmidt, W. K. H., Simon, M., and Spiegelhauer, H. 1979, Space Science Instrumentation, 4, 303.
- Balasubrahmanyam, V. K., Arens, J. F., Ormes, J. F., Siohan, F., Yodh, G. B., Schmidt, W. K. H., Simon, M., and Spiegelhauer, H. 1979, Proc. 16th Intl. Cosmic Ray Conf., Kyoto, Japan.
- Balasubrahmanyam, V. K., and Ormes, J. F. 1973, Ap. J., 186, 109.
- Caldwell, J. H. 1977, Ap. J., 218, 269.
- Garcia-Munoz, M., Mason, G. M., and Simpson, J. A. 1977, Proc. 15th Intl. Cosmic Ray Conf., Plovdiv 1, 224.
- Goodman, J. A., Ellsworth, R. W., Ito, A. S., MacFall, J. R., Siohan, F., Streitmatter, R. E., Tonwar, S. C., Vishwanath, P. R., and Yodh, G. B. 1979, Phys. Rev. Lett. 42, 854.
- Jones, W. V. 1976, Nuclear-Electromagnetic Cascade Monte-Carlo Simulation Program, GSFC internal memo.
- Jones, W. V., Ormes, J. F., Schmidt, W. K. H. 1977, Nucl. Inst. and Methods, 140, 557.
- Juliusson, E. 1974, Ap. J., 191, 331.
- Lezniak, J. A., and Webber, W. R. 1978, Ap. J., 233, 676.
- Lezniak, J. A., and Webber, W. R. 1979, Ap. J., in press.
- Maehl, R. C., Ormes, J. F., Fisher, A. J., and Hagen, F. A. 1977, Ap. Space Science, 47, 163.
- Ormes, J. F., and Freier, P. S., 1978, Ap. J., 222, 471.
- Orth, C. D., Buffington, A., Smoot, G. F., and Mast, T. S. 1978, Ap. J., 226, 1147.
- Saito, T., Sato, A., Sugimoto, H., Matsubayashi, T., and Noma, M., 1974, J. Phys. Soc. Japan, 37, 1462.

- Schmidt, W. K. H., Atallah, K., Cleghorn, J. F., Jones, W. V., Modlinger, A.,
and Simon, M 1976, *Astronomy and Astrophys.*, 46, 49.
- Shapiro, M. M., Silberberg, R., and Tsao, C. H. 1973, 13th Intl. Cosmic Ray
Conf., Denver, 1, 578.
- Shapiro, M. M., Silberberg, R., and Tsao, C. H. 1975, 14th Intl. Cosmic Ray
Conf., Munich, 2, 532.
- Silberberg, R., and Tsao, C. H. 1973, *Ap. J. Suppl.*, 25, 315 and 335.
- Silberberg, R., and Tsao, C. H. 1977, *Proc. 15th Intl. Cosmic Ray Conf., Plovdiv*,
2, 84 and 89.
- Westfall, G. D., Wilson, L. W., Lindstrom, P. J., Crawford, H. F., Greiner, D. E.,
and Heckman, H. H. 1978, LBL-7162 submitted to *Phys. Rec. C*.
- Yodh, G. B. 1977, Private communication.



GERMAN-AMERICAN HIGH ENERGY COSMIC RAY TELESCOPE

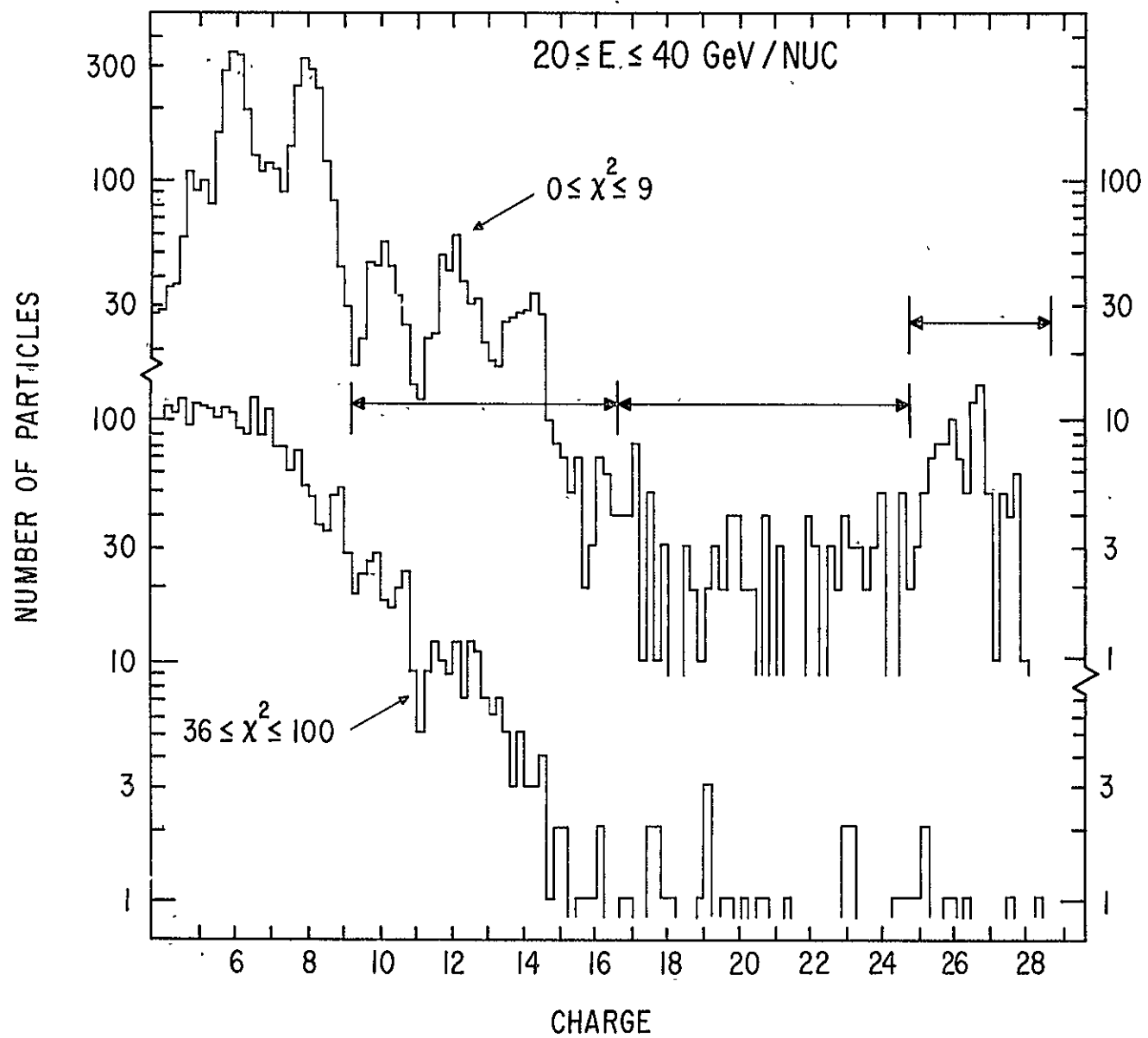


Fig. 2

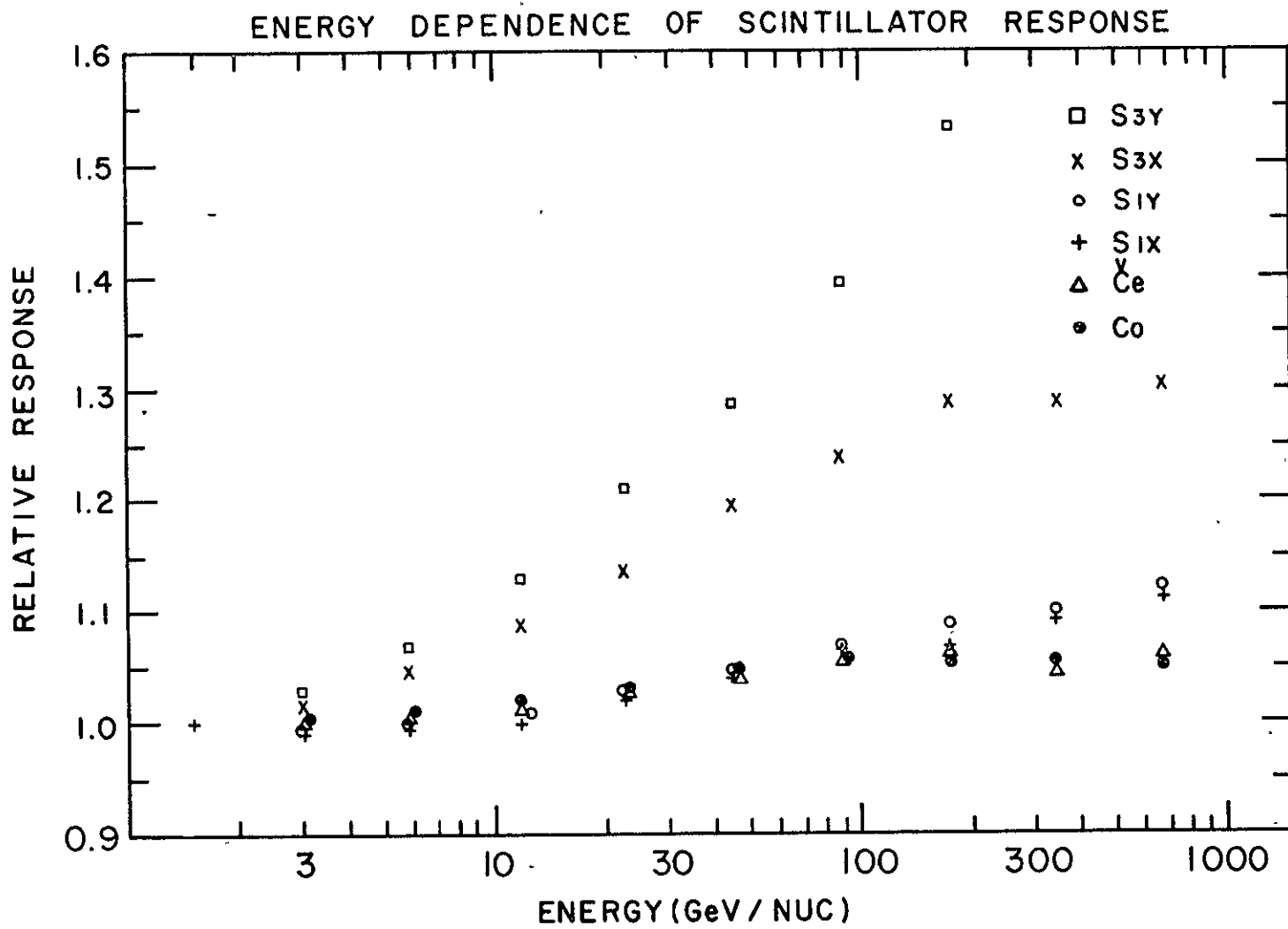


Fig. 3

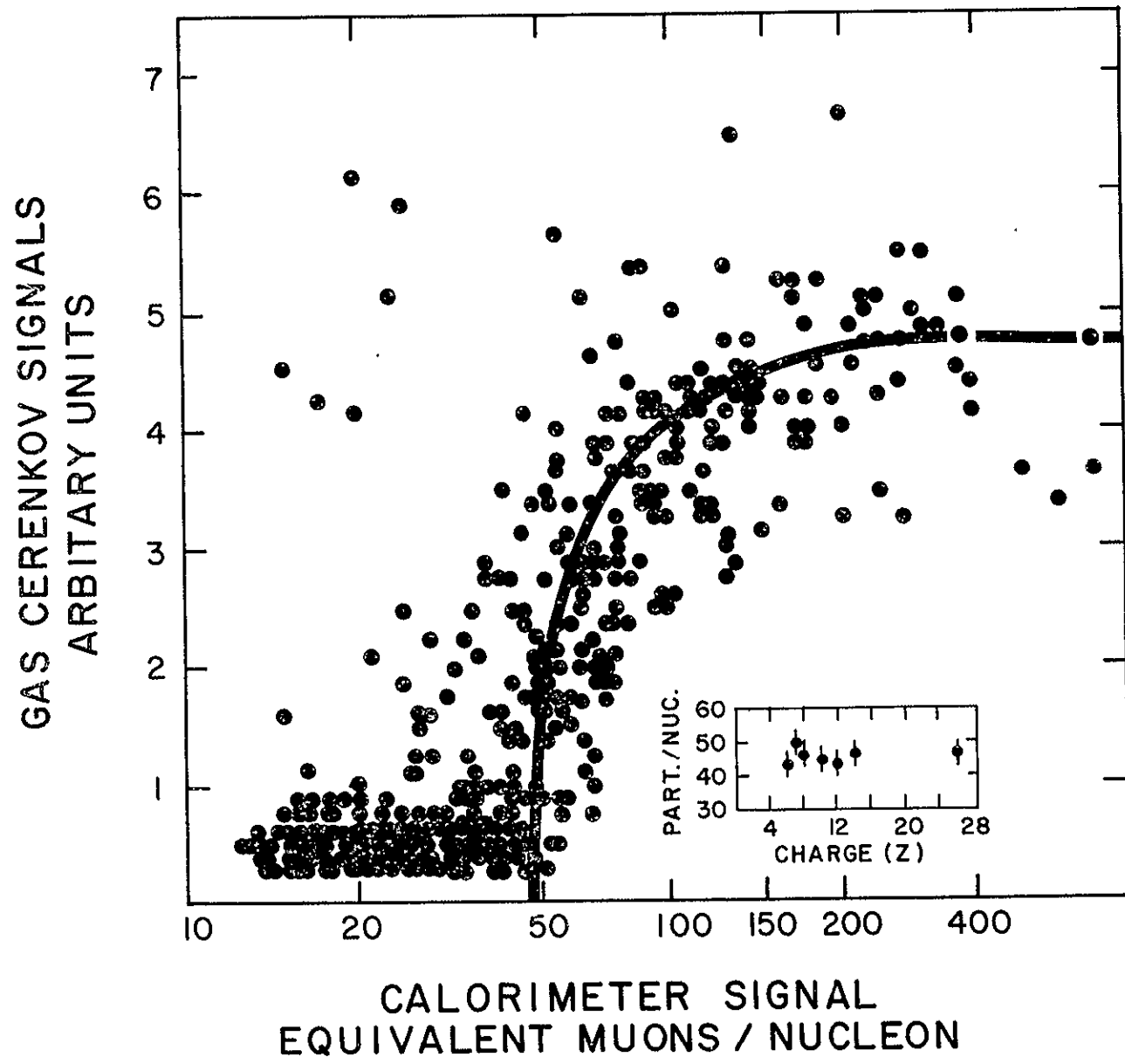


Fig. 4

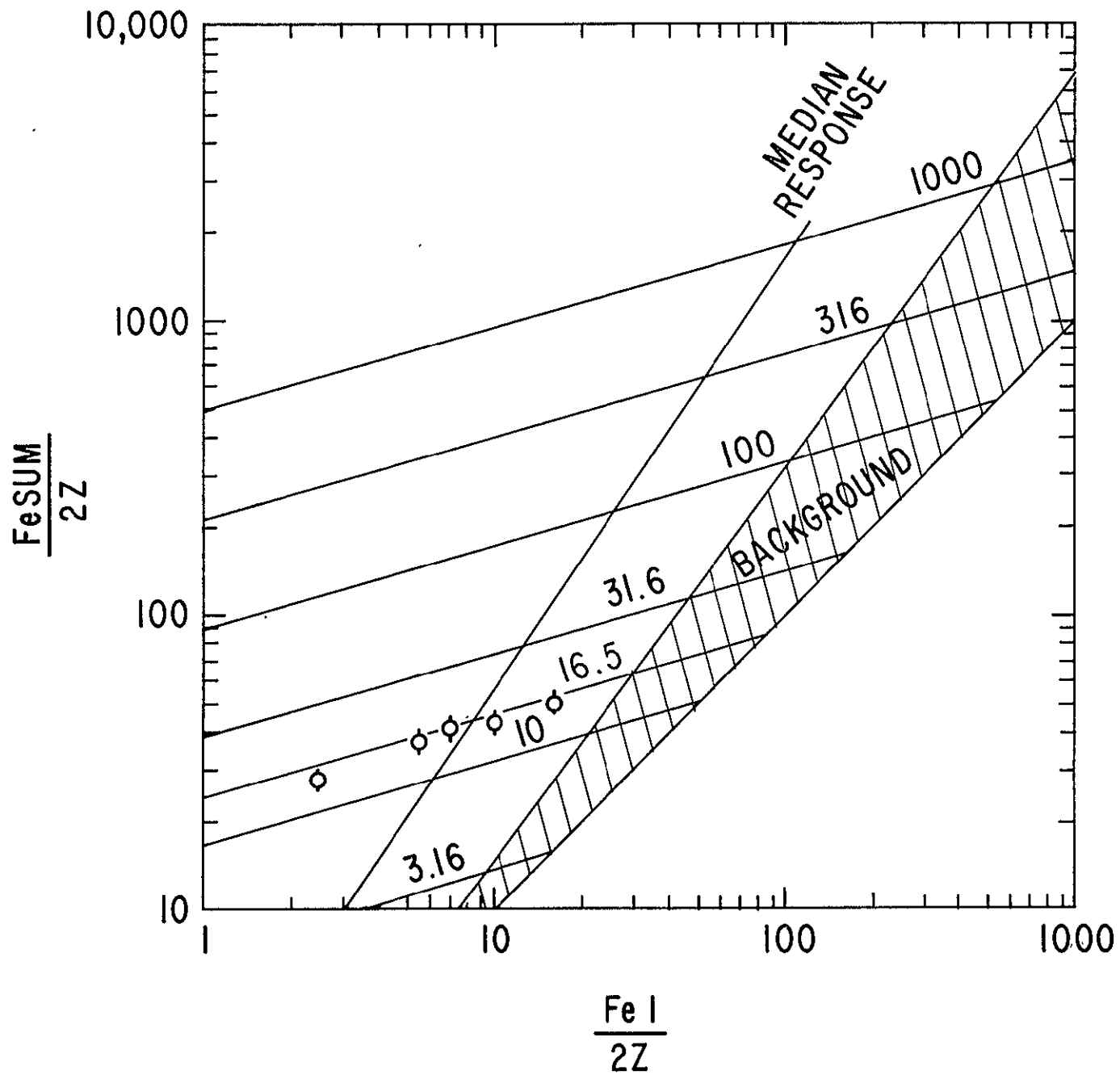


Fig. 5

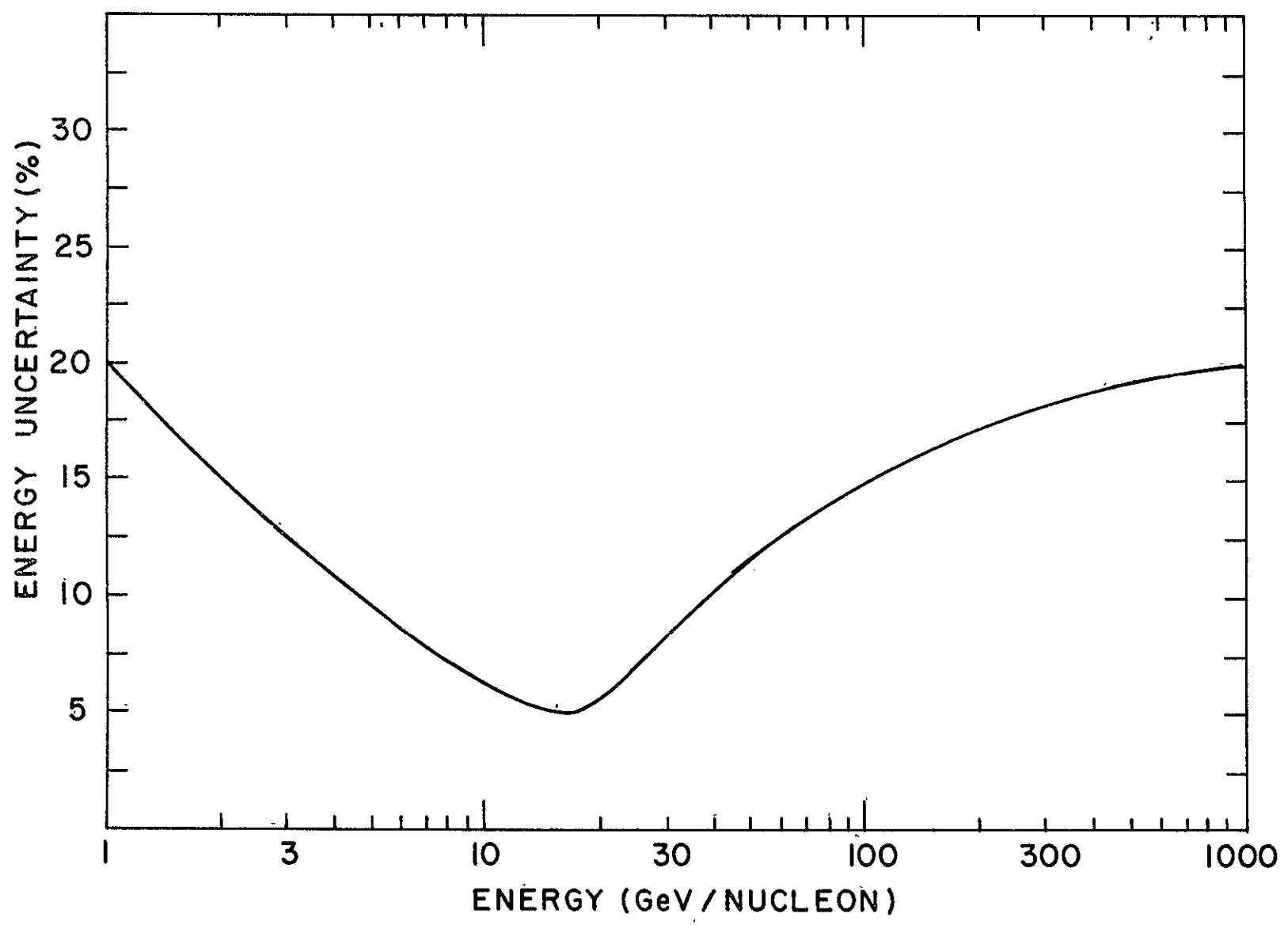


Fig. 6

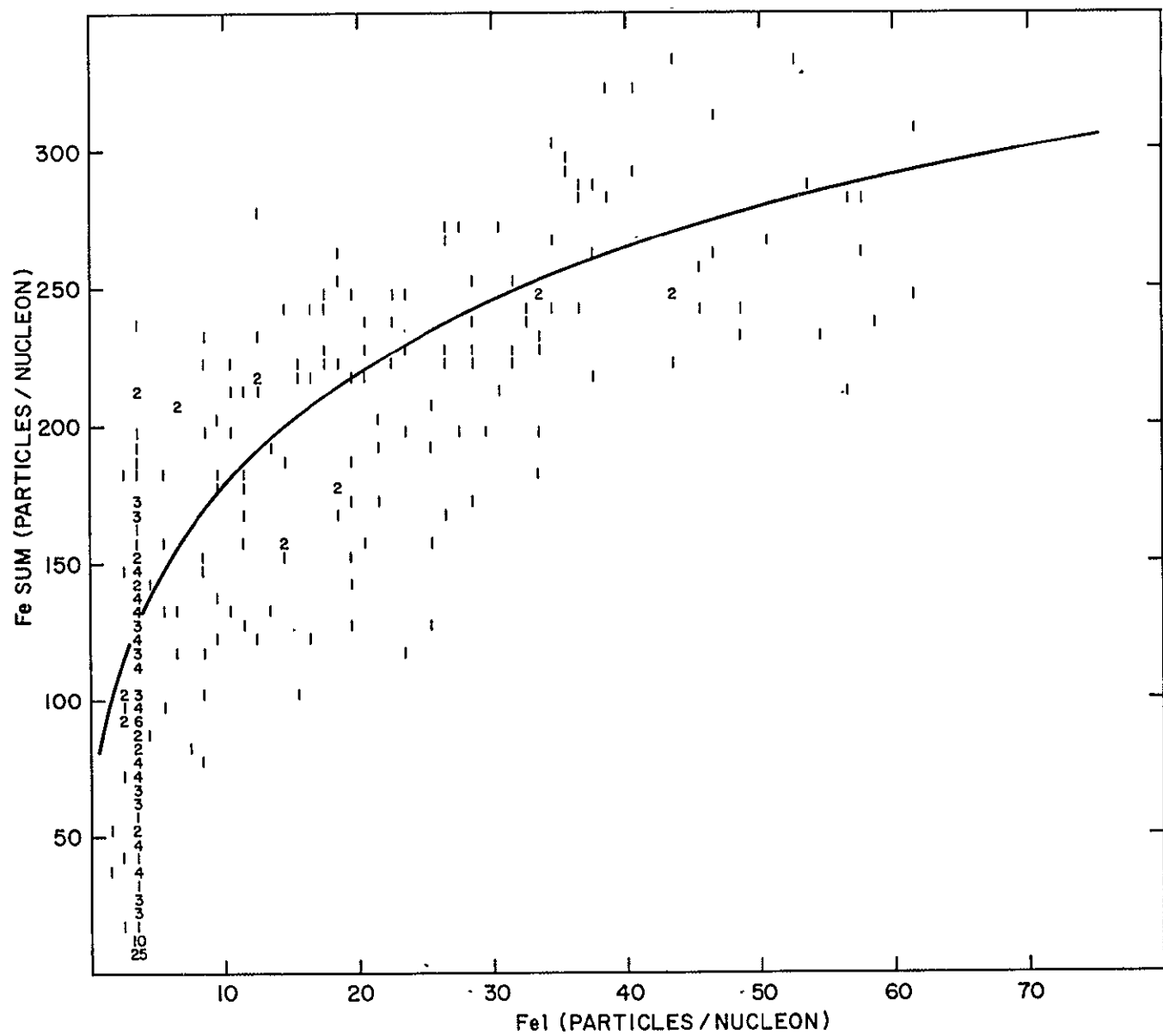


Fig. 7

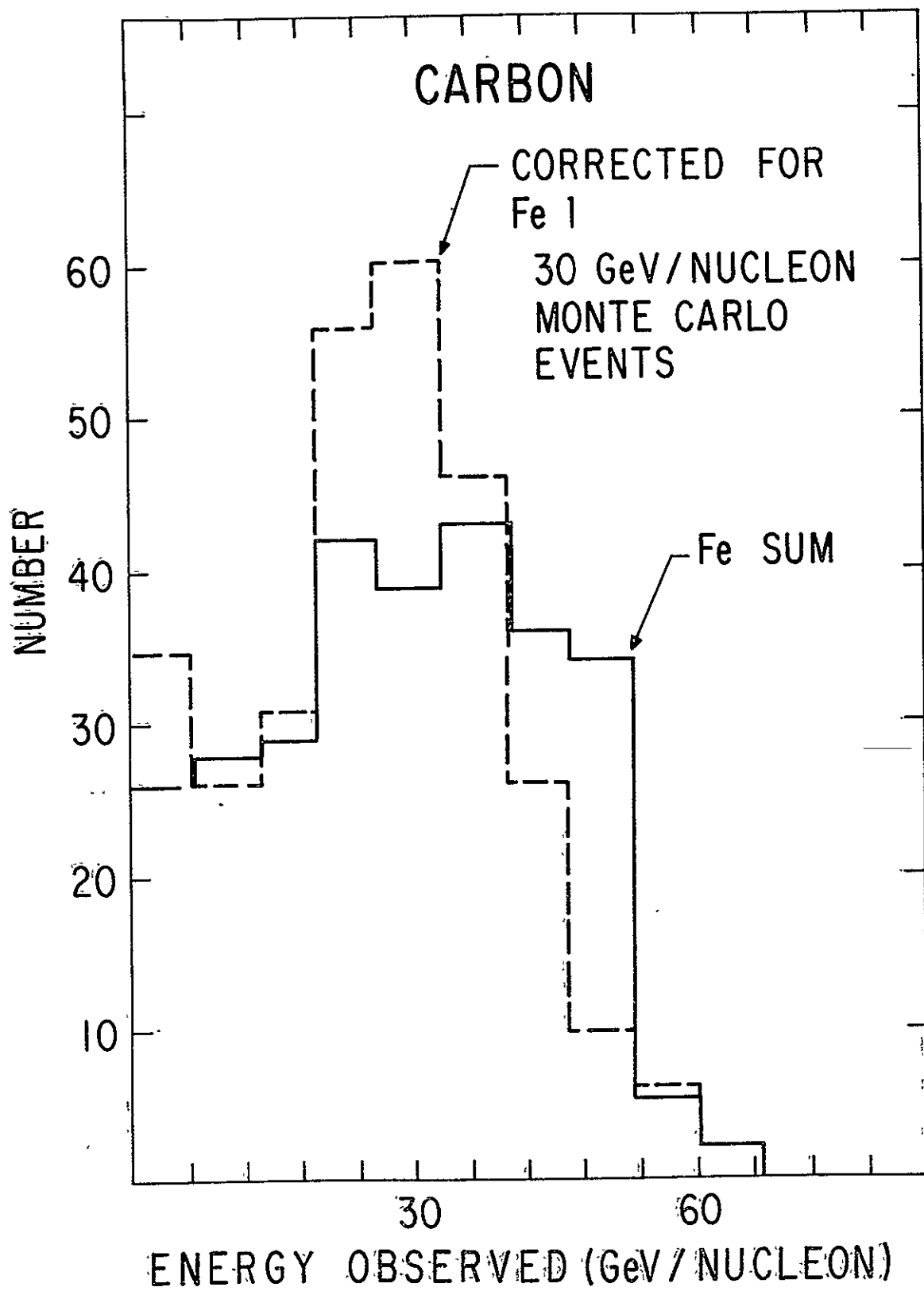


Fig. 8

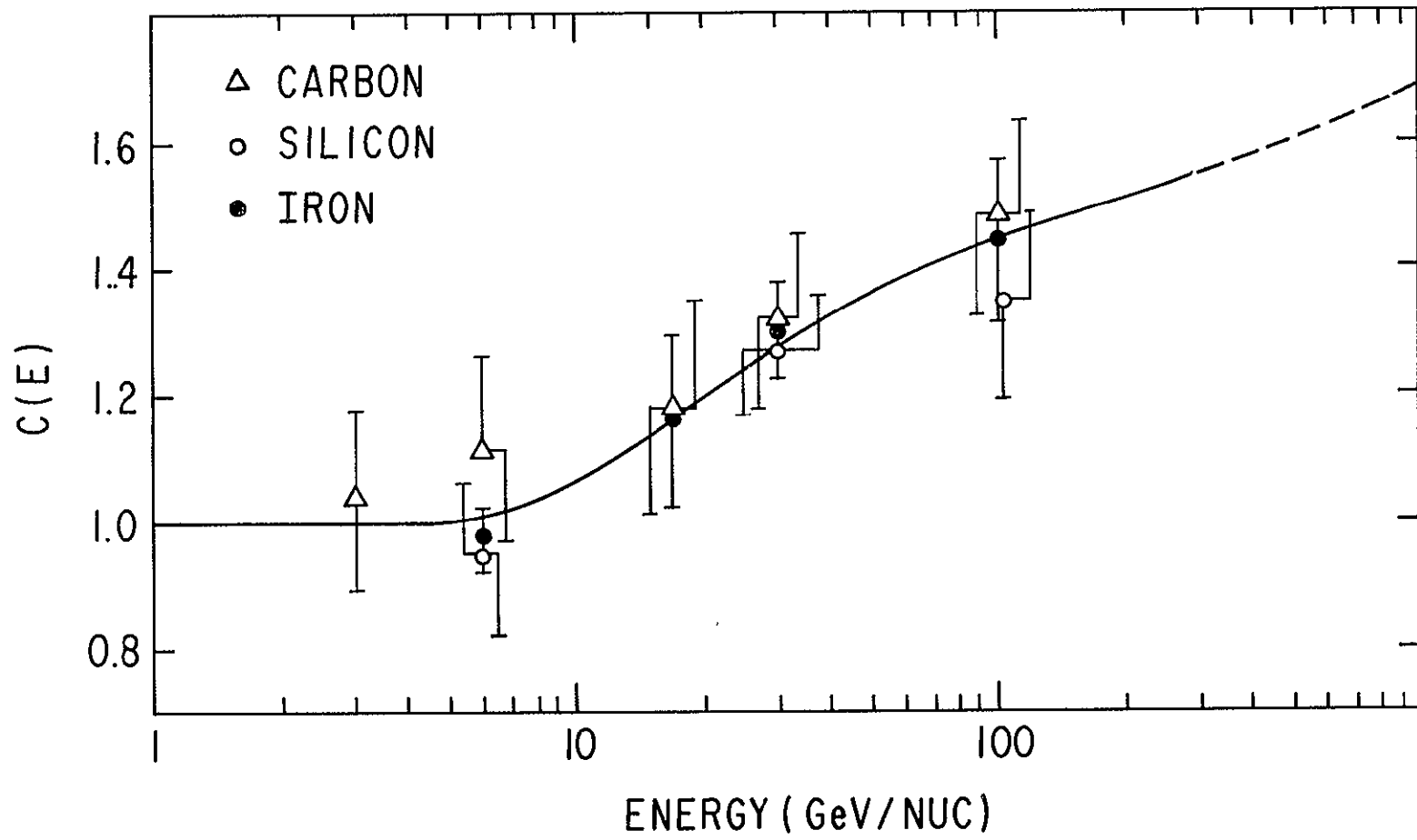


Fig. 9

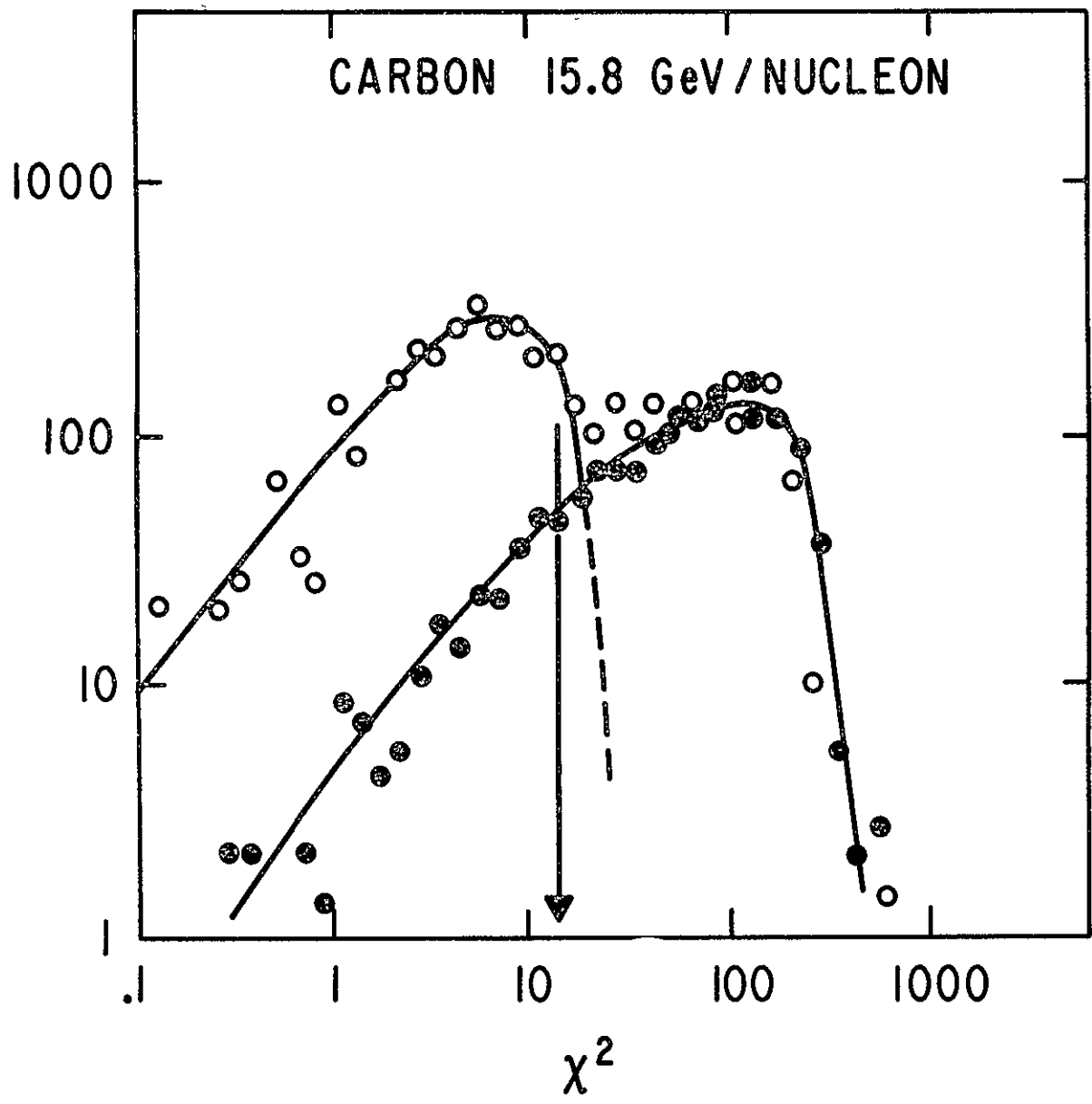


Fig. 10.

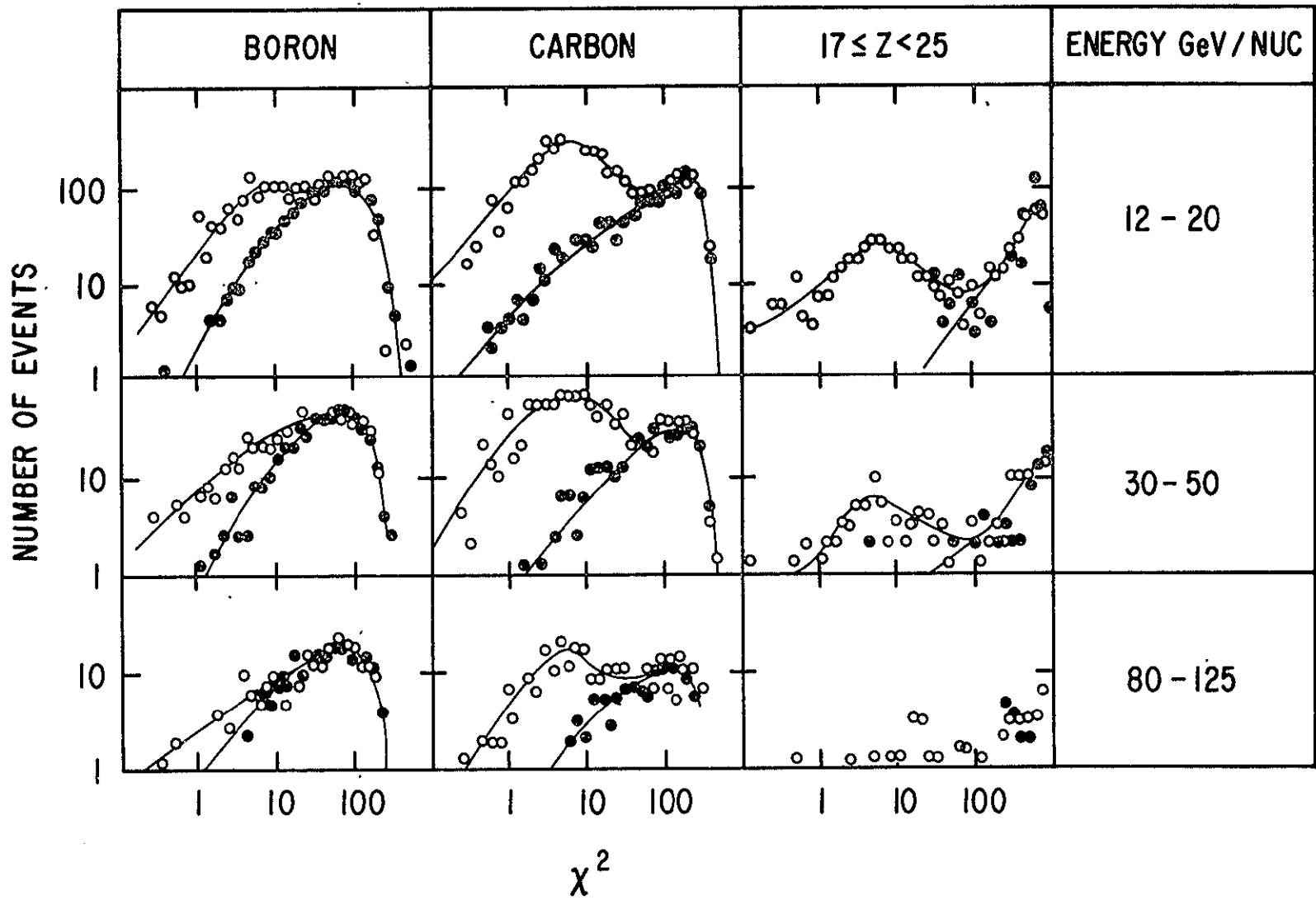


Fig. 11

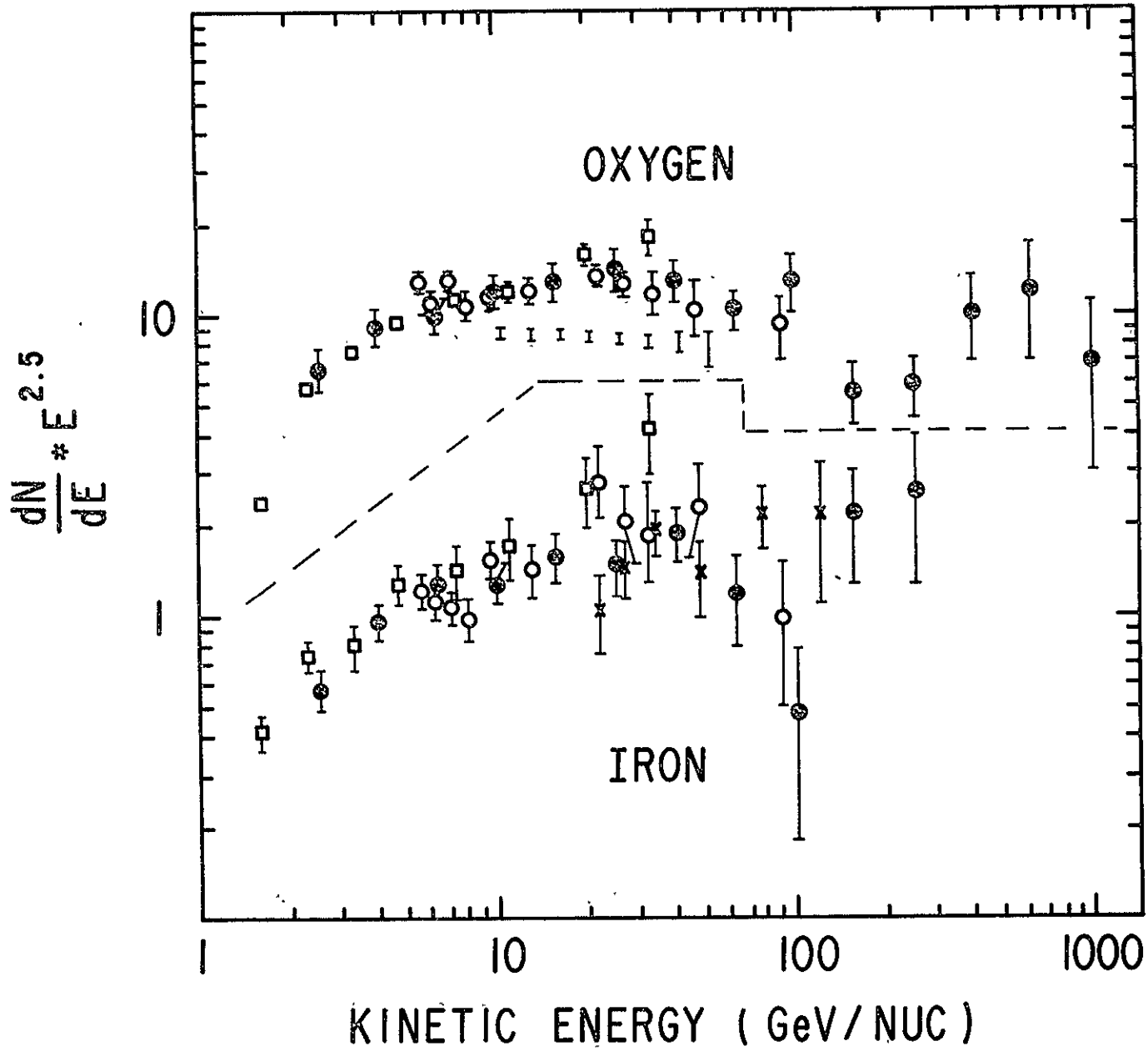


Fig. 12

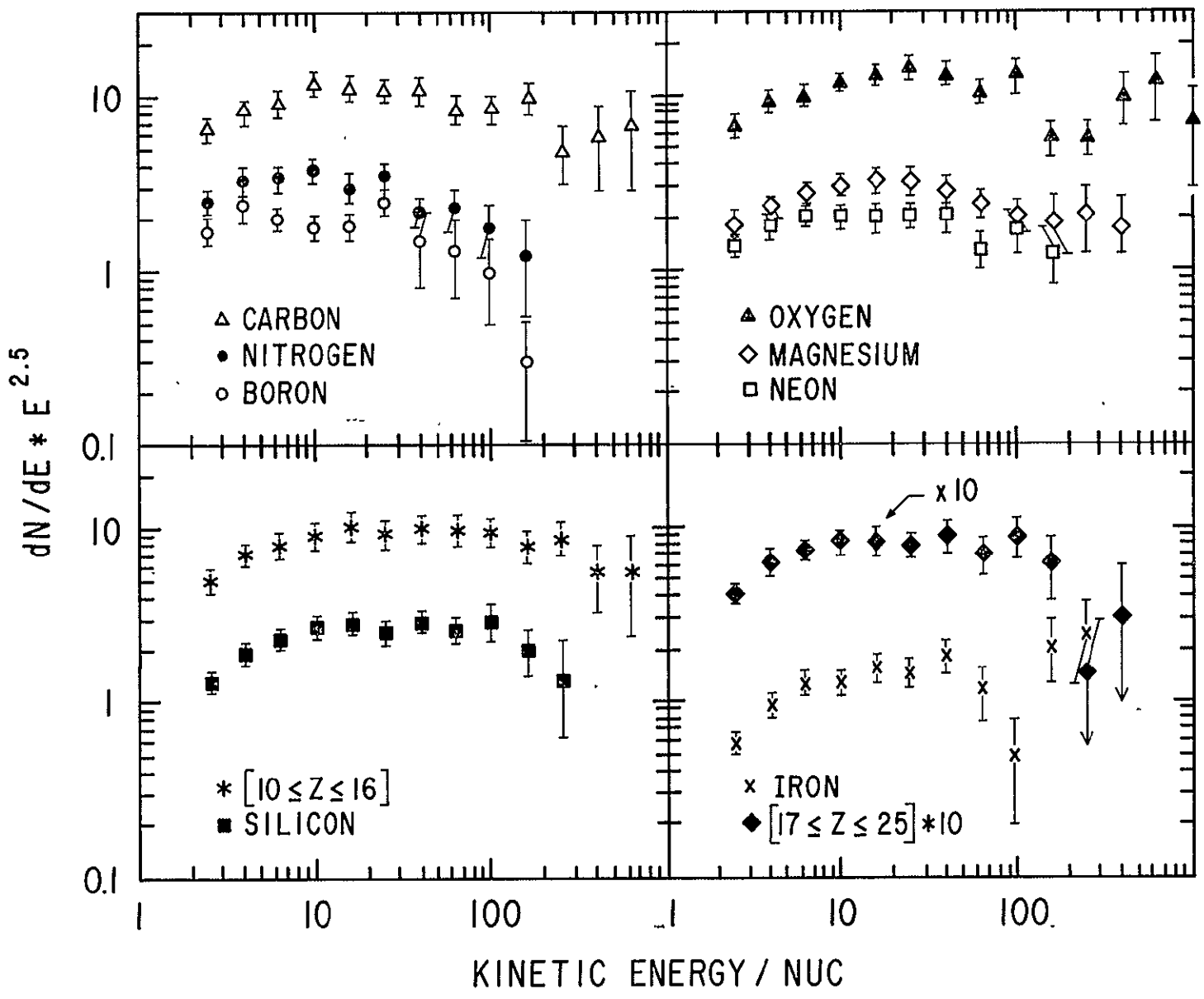


Fig. 13

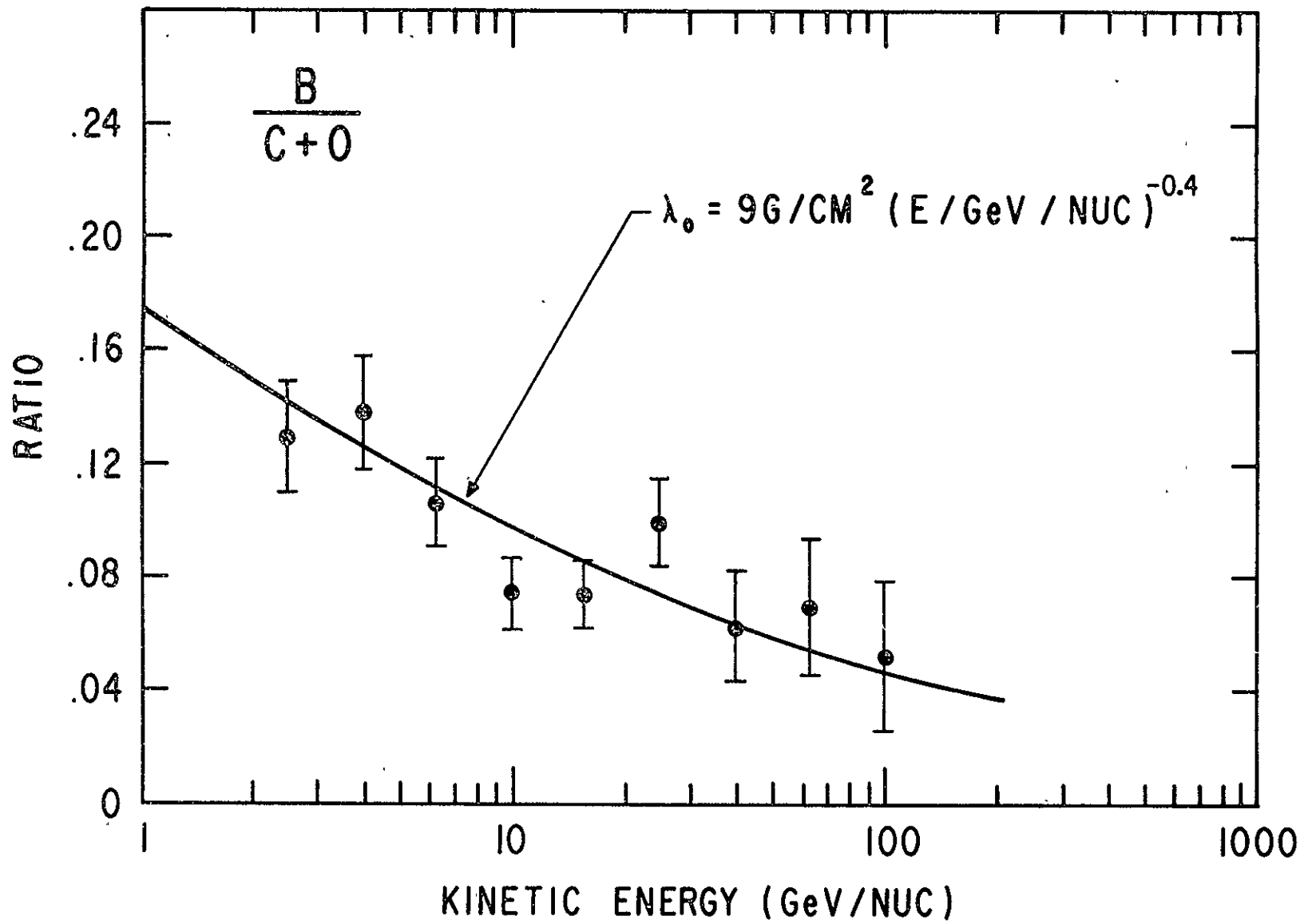


Fig. 14

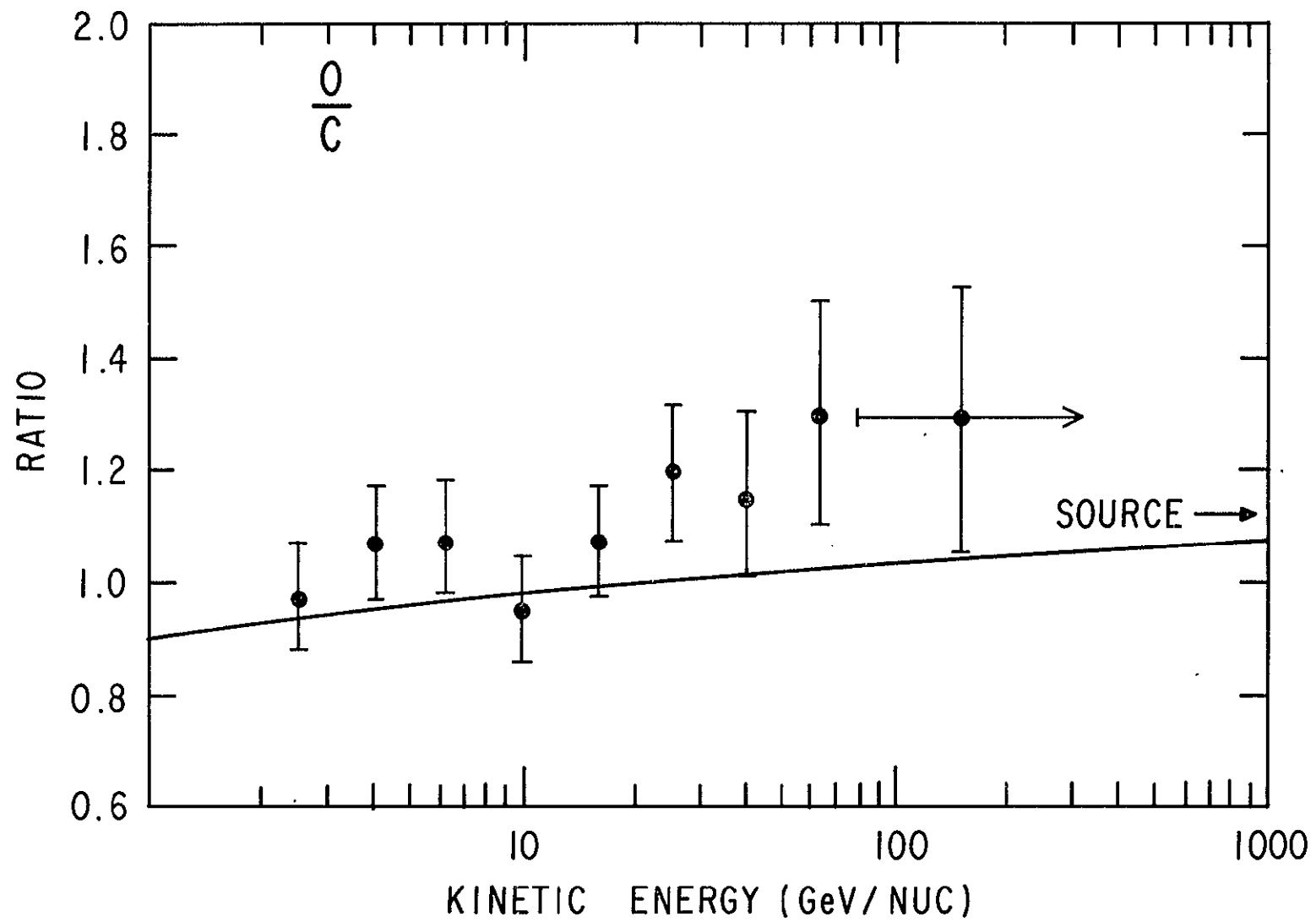


Fig. 15

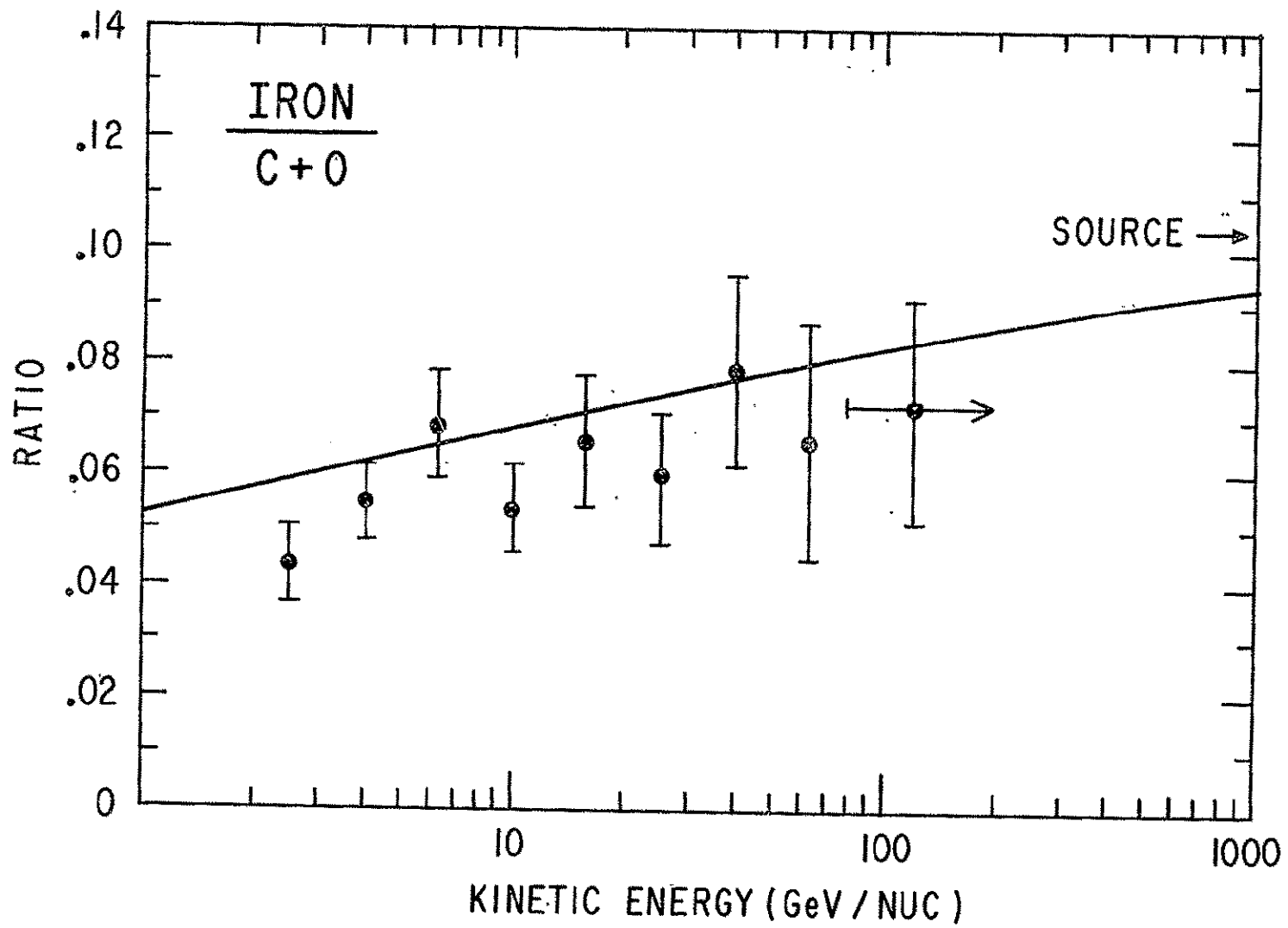


Fig. 16

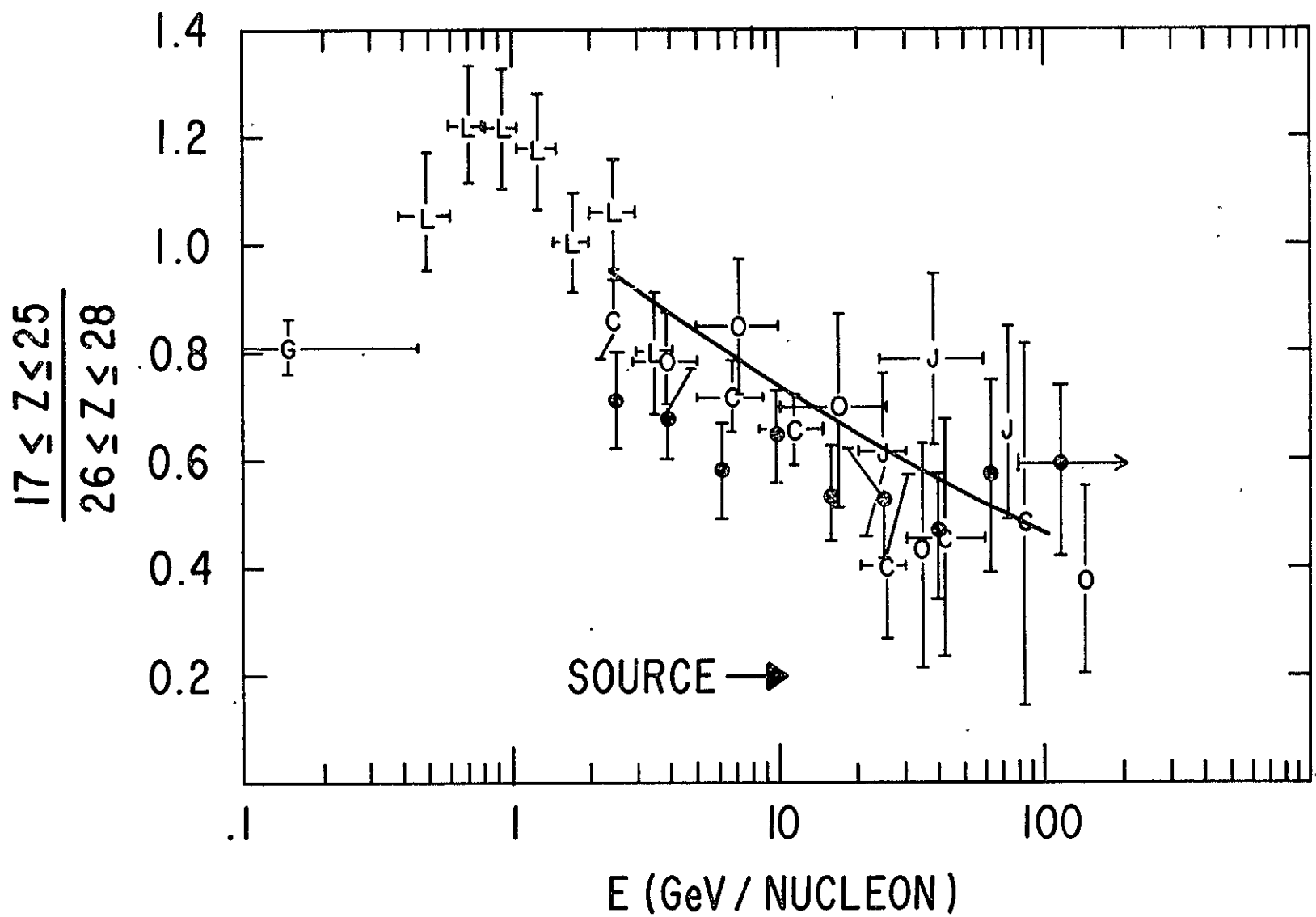


Fig. 17

BIBLIOGRAPHIC DATA SHEET

1. Report No. TM 80587	2. Government Accession No.	3. Recipient's Catalog No.	
4. Title and Subtitle Energy Spectra of Cosmic Ray Nuclei to Above 100 GeV/Nucleon		5. Report Date October 1979	
		6. Performing Organization Code 660	
7. Author(s) M. Simcn, H. Spiegelhauer, W. Schmidt, F. Siohan, J. Ormes, V. Balasubrahmanyam, J. Arens		8. Performing Organization Report No.	
9. Performing Organization Name and Address Cosmic Radiations Branch Laboratory for High Energy Astrophysics NASA/Goddard Space Flight Center Greenbelt, MD 20771		10. Work Unit No.	
		11. Contract or Grant No.	
		13. Type of Report and Period Covered	
12. Sponsoring Agency Name and Address		14. Sponsoring Agency Code	
15. Supplementary Notes To be printed in Astrophysical Journal			
16. Abstract Energy spectra of cosmic ray nuclei boron to iron have been measured from 2 GeV/nucleon to beyond 100 GeV/nucleon. The data were obtained using an ionization calorimeter flown on a balloon from Palestine, Texas. The 3450kg payload floated at 7g/cm ² for almost 24 hours. The results are in excellent agreement with those of other workers where overlaps exist. The spectra are not consistent with single power laws and demonstrate the power of using a single technique sensitive over a large dynamic range. The data are consistent with the leaky box model of cosmic ray propagation. The boron data indicate that the cosmic ray escape length decreases with increasing energy as $E^{-(0.4 \pm 0.1)}$ up to 100 GeV/nucleon. Secondary nuclei from iron are also consistent with this dependence. Predicted changes in the energy dependence of the ratios of primary nuclei O/C and IRON/C+O are also observed.			
17. Key Words (Selected by Author(s)) cosmic rays, abundances, energy spectra, leaky box propagation		18. Distribution Statement	
19. Security Classif. (of this report) UN	20. Security Classif. (of this page)	21. No. of Pages	22. Price*